# *Electronic Supporting Information*

# Direct *in situ* measurement of specific capacitance, monolayer tension, and bilayer tension in a droplet interface bilayer

*Graham J. Taylor, Guru A. Venkatesan, C. Patrick Collier, Stephen A. Sarles**

[*] Stephen A. Sarles
Bioinspired Materials and Transduction Laboratory
Department of Mechanical, Aerospace & Biomedical Engineering
University of Tennessee, Knoxville
Knoxville, TN 37996
E-mail: ssarles@utk.edu

**CONTENTS**

## PENDANT DROP MONOLAYER TENSION MEASUREMENTS

Due to the extremely low interfacial tension (≤1 mN/m) achieved by lipid monolayer self-assembly, a pendant drop of aqueous lipid solution formed at the tip of a needle in oil often falls off, making it hard to measure the equilibrium tension. This is particularly problematic when the effects of gravity are significant, for instance when testing with hexadecane which has a much lower density than the aqueous phase ($\rho_{hexadecane}$=0.77 g/mL compared to $\rho_{buffer}$=1.00 g/mL). To circumvent this problem, a J-shaped needle is used to form an oil drop in the lipid aqueous solution as shown in Figure S1A. A glass cuvette is thoroughly cleaned by rinsing in acetone, IPA, and then deionized water before placing the cuvette in an oven (80°C) for several minutes or until it is fully dry. Clean, dry cuvettes are filled with 2 mL of liposome solution ($\rho$ = 1.0007 g/mL). A clean 23 gauge steel needle (Ramé-Hart) is bent to form the J-shaped dispensing tip, taking care to ensure that the tip of the needle will be vertically oriented once assembled onto the goniometer. After fitting the needle on the automatic dispenser, few μL of the appropriate oil mixture is drawn into the needle. In order to prevent wetting of oil on the needle's exterior surface, the tip of the needle is dabbed with a clean wipe (Kimwipe) to remove residual oil before lowering the needle into the cuvette such that the tip is fully submerged into the aqueous solution. A 1 μL drop of the oil mixture is dispensed at the tip of the needle and the interfacial tension measurement begins. Example tension data from a representative experiment is included in Figure S1B. Measurements are taken at a rate of 60 samples per minute until an equilibrium value is reached. All measurements are performed at room temperature.

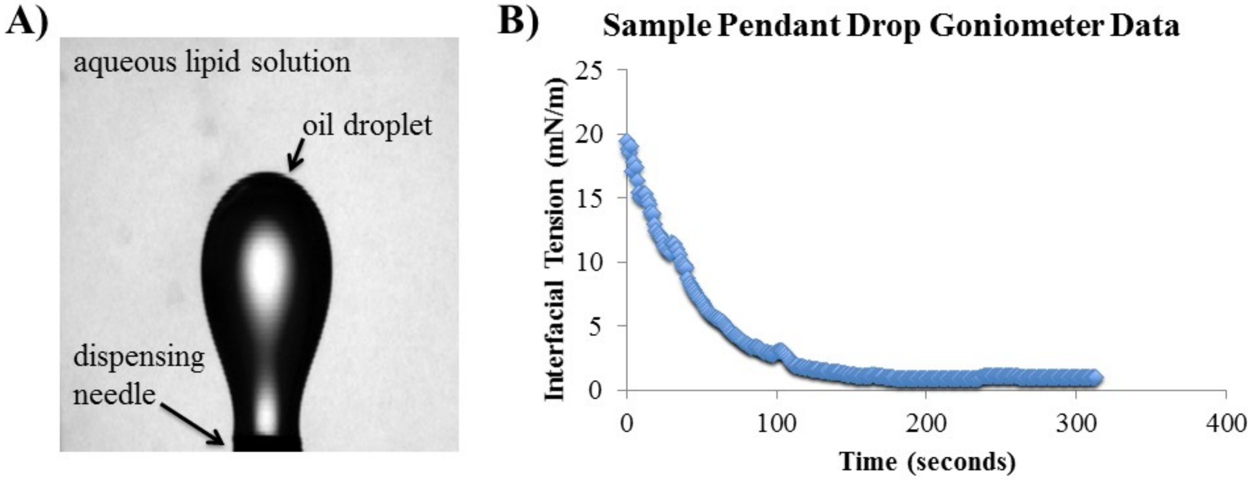

**Figure S1.** A) Representative image of the pendant droplet formed during goniometer measurements of lipid monolayer surface tension. An inverted 1 μL droplet of oil (the less dense liquid phase) is dispensed at the tip of a J-shaped needle submerged in aqueous solution containing small unilamellar liposomes (DPhPC or DPhPC:cholesterol). The droplet "floats" upwards as a result of the difference in the oil and aqueous phase densities. B) Typical response of monolayer tension upon creating of a new clean, lipid-free oil droplet at the tip of the dispensing needle. Tension decreases instantaneously upon droplet formation, settling to a steady state value as lipid self-assembly and packing reach equilibrium. Steady state monolayer tensions are typically near 1 mN/m. Typical test results resemble the example shown in which 62% of the overall tension decrease occurs over a period of 30-40 seconds.

## DROPLET SAGGING DUE TO GRAVITY

Specific capacitance measurements involve area calculations that are affected by the shape and circularity of a DIB interface. The extent of gravity-driven droplet deformation is investigated experimentally by performing specific capacitance measurements in hexadecane with pipetted droplets of different sizes. Droplets are pipetted onto the agarose-coated ball-ended electrodes as usual in these experiments, and specific capacitance measurements made on multiple newly formed (symmetric) DIBs with droplet volumes ranging from 200 nL to 500 nL. Figure S2A shows images of DIBs formed from aqueous droplets of varying volume in hexadecane. These "bottom view" images are obtained through the microscope objective directly below the drops. Images are processed to determine the bilayer contact length which is a principal diameter, $a$. If the interface is assumed to be circular, the area of the interface is then calculated by:

$$A = \pi a^2 / 4 \qquad \text{Equation S1}$$

$C_M$ values are calculated for each trial using a circular area assumption. Figure S2B shows the average specific capacitance value as a function of droplet volume (error bars represent ± one standard deviation). It is clear that specific capacitance values are increasing with droplet volume despite the fact that the thickness and dielectric permittivity of the lipid bilayer should be insensitive to the macroscale droplet size. However, the observed increase in $C_M$ with droplet size is explained by considering droplet deformation due to gravity. There are two dominant forces that determine droplet shape: gravity and

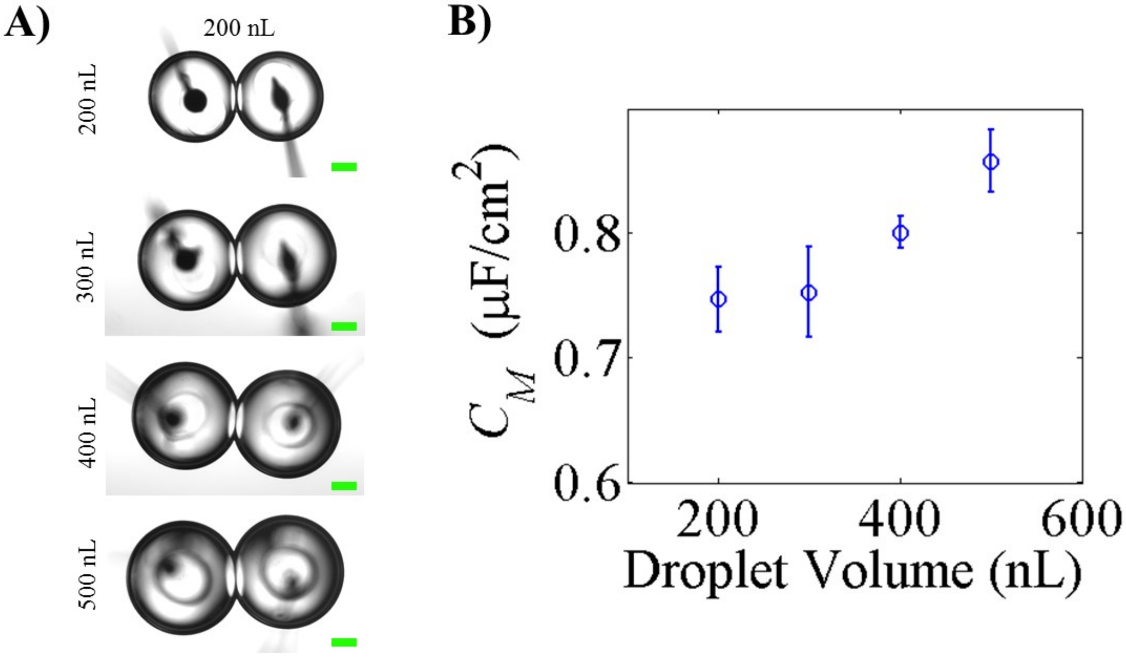

**Figure S2.** A) DPhPC DIBs formed in hexadecane using droplets with volumes of 200, 300, 400, and 500 nL. Images are used to determine the bilayer contact length $a$. Green scale bars represent 100 μm. B) Specific capacitance ($C_M$) as a function of droplet size, calculated via the method of dynamically varying area as described in the manuscript (error bars represent ± one standard deviation; see Table S1). For the results shown here, the bilayer is assumed to be circular with area determined by $A=\pi a^2/4$.

surface tension. For small droplets with low Bond numbers, the effects of gravity become negligible and surface tensions typically dominate. However, when interfacial tensions are also very low or when droplets are large, the droplet shape is affected by surface tension and gravity. It should be noted that with our method as described, the bottom-up view through the microscope provides viewing access of the bilayer diameter from only one direction. If droplets are contained in a less dense oil phase, then they will sag in the vertical direction. Thus, the contact length obtained from bottom view images represents the minor axis (*a*) of an ellipse whose major axis is being stretched by gravity. In these cases, the actual bilayer area is in fact larger than what would be calculated if the bottom-up diameter is used along with the assumption that the bilayer profile is circular. The result is that specific capacitance, taken as capacitance divided by area, is artificially high when droplets sag and circular area equations are employed.

**Table S1.** Summary of $C_M$ obtained in DIB trials with varying droplet volume assuming a perfectly circular interface.

| | **Drop Volume** | | | |
|---|---|---|---|---|
| | **200 nL** | **300 nL** | **400 nL** | **500 nL** |
| $C_M$ | 0.741<br>(0.028)<br>*n*=8 | 0.753<br>(0.036)<br>*n*=13 | 0.801<br>(0.013)<br>*n*=7 | 0.828<br>(0.017)<br>*n*=2 |
| correction factor | 1.1585 | 1.1773 | 1.2519 | 1.3413 |

*values from tests performed using DPhPC in pure hexadecane

## EXPERIMENTAL AND COMPUTATIONAL DETERMINATION OF ELLIPTICITY FACTORS

Previously reported values for $C_M$ can be used to calculate a correction factor for each droplet volume based on the experimentally observed values in Table S1. The correction factor is derived from the geometry of the interface as it assumes a non-circular profile due to droplet deformation. A sagging droplet has a major axis diameter that is longer than the minor axis diameter obtained from images. Assuming the interface to take the form of an ellipse, the area is now calculated by:

$$A = \pi ab/4 \qquad \text{Equation S2}$$

We introduce an ellipticity factor, $\varepsilon$, that represents the ratio of the major axis diameter (*b*) to the minor axis diameter (*a*).

$$\varepsilon = \frac{b}{a} \qquad \text{Equation S3}$$

Rearranging and substituting Equation S3 into Equation S2 yields the area of the elliptical interface in terms of only the minor axis diameter and the ellipticity factor.

$$A = \pi a(\varepsilon a)/4 = \varepsilon(\pi a^2/4) \qquad \text{Equation S4}$$

While we do not directly observe the major axis diameter of sagging droplets, we are able to calculate ellipticity factors by dividing our artificially high values of $C_M$ by an accepted value (0.64 μF/cm$^2$, DPhPC, hexadecane).[3, 4] The resulting volume-specific ellipticity factors are shown in Table S1.

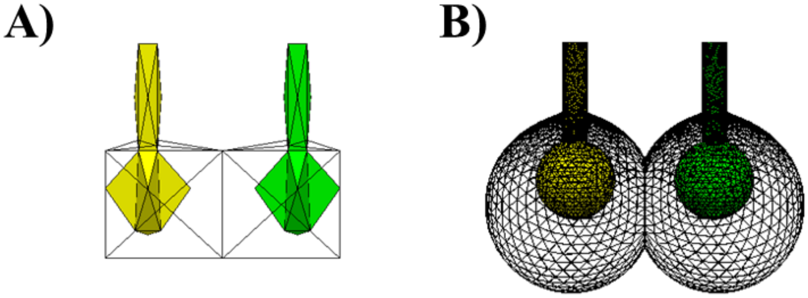

**Figure S3.** Representative images showing a DIB (A) before, and (B) after evolving. The simulation is performed using Surface Evolver, a computer program that simulates interfacial behavior by minimizing the free energy of defined surfaces. A) Initial surface structure defining the electrodes (one yellow and one green) and the water droplets. B) An image saved after evolving the DIB with monolayer tension set to 1 mN/m, bilayer contact angle at 25°, electrode spacing of 0.7 mm, and 300 nL droplet volumes.

Surface Evolver[5] is a computer program that has been used to simulate the behavior of droplets and foams.[6] The program operates by minimizing the free energy of surfaces created using defined vertices, edges, and facets, and it is employed here to further quantify droplet deformation as a function of the difference in droplet and oil densities. Figure S3 shows the results of an evolution from initially defined surfaces (Fig S3A) to a suspended DIB (Fig. S3B) with the droplets in wireframe and the electrodes colored green and yellow. The model used includes gravity and allows for changing the density of the droplet and the oil phase. Certain parameters are fixed during each evolution including the monolayer tension at the oil-water interface (1 mN/m for all), the tension between the electrode and the oil (5mN/m for all), the droplet volume, and the equilibrium contact angle. Each droplet is confined to the electrode along the cylindrical portion such that the ball tip remains fully encapsulated by the droplet.

To assist determination of shape ellipticity factors for specific capacitance area calculations, we investigate the effects of varying density differences by performing a series of evolutions while changing the density difference to represent fractions of silicone oil ranging from 0 to 100%. Figure S4A-B shows images saved after separate evolutions with varying oil compositions. Figure S4A shows a side view of the DIB at each extreme: pure hexadecane (top) and pure silicone oil (bottom). Figure S4B shows the bilayer region for 100%, 80%, 60%, 40%, 20%, and 0 % hexadecane volume fractions as indicated above each image. Similarly, the density difference between the water and oil mixture for each case is displayed below each respective image. The interface formed in pure hexadecane ($\rho_{\mathrm{hexadecane}}$=0.77 g/mL) is clearly sagging in the vertical direction. As expected, this ellipticity diminishes as the oil mixture is loaded with dense silicone oil. The coordinates of the equilibrium bilayer are exported to MATLAB to further analyze bilayer area and its geometry. Ellipticity is quantified by extracting the minor ($a$) and major ($b$) axis diameters as illustrated in Figure S4C. Ellipticity can then be monitored as a function of oil composition by evaluating the quantity $\varepsilon_{b/a}=b/a$ which increases from unity as the droplets sag and extend the bilayer major axis. Figure S5A shows calculated values of $\varepsilon_{b/a}$ as a function of the difference in the density of the droplet and the oil mixture with evolutions using 300 nL droplets and a 25° equilibrium contact angle (half-bilayer angle). Clearly, the interface transitions from being vertically distended and elliptical to nearly circular as the silicone oil content increases and the density difference decrease. Identical results

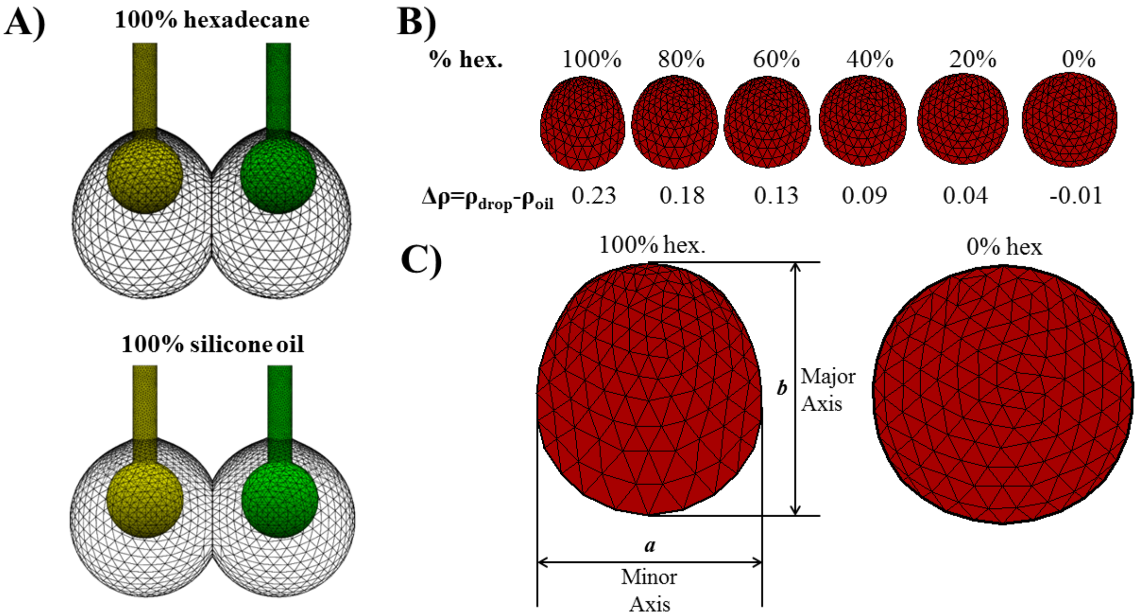

**Figure S4.** A) DIBs after evolution in Surface Evolver. Top – the oil phase is pure hexadecane, and droplets are seen to sag downwards. Bottom – the oil phase is pure AR 20 which is more dense than water. B) Images of the bilayer region alone after Surface Evolver trials with 300 nL droplets and varying ratios of silicone oil: hexadecane. The difference between the density of the aqueous droplet and the oil mixture is shown. C) Magnified versions of the images in (B) representing pure hexadecane (left) and AR 20 silicone oil (right).

are obtained in other evolution trials using a 45° contact angle (Figure S5B), thus it is not expected that conclusions drawn from Surface Evolver analysis are heavily affected by the selection of contact angle (at least in the typical range of around 25-45°).

The values obtained for $\varepsilon_{b/a}$ provide both a) information regarding the shape of the bilayer, and also b) the ellipticity factors required to confidently estimate the bilayer area using the minor axis diameter alone. The ability to calculate area using the minor axis diameter enables more accurate estimation of area in experiments with images taken from beneath the suspended droplets through an inverted microscope. All experimental tests in the manuscript are performed using 300 nL drops, and the same pipette is used for consistency. To calibrate Surface Evolver calculations, we compared the volume-specific ellipticity factor (Table S1) obtained from DIBS formed with 300nL droplets to values of ellipticity for varying droplet volumes computed in Surface Evolver. This comparison shows that the experimentally observed ellipticity is most closely reproduced by Surface Evolver calculations when using 400nL droplets. To our knowledge, there are no published values of $C_M$ for planar bilayers or DIBs formed in mixtures of hexadecane and AR20 silicone oil, thus Surface Evolver is used to compute ellipticity factors for 400 nL droplets with the density difference adjusted to match each oil combination tested. The final ellipticity factors used in area calculations for specific capacitance measurements provided in the manuscript are listed in Table S2.

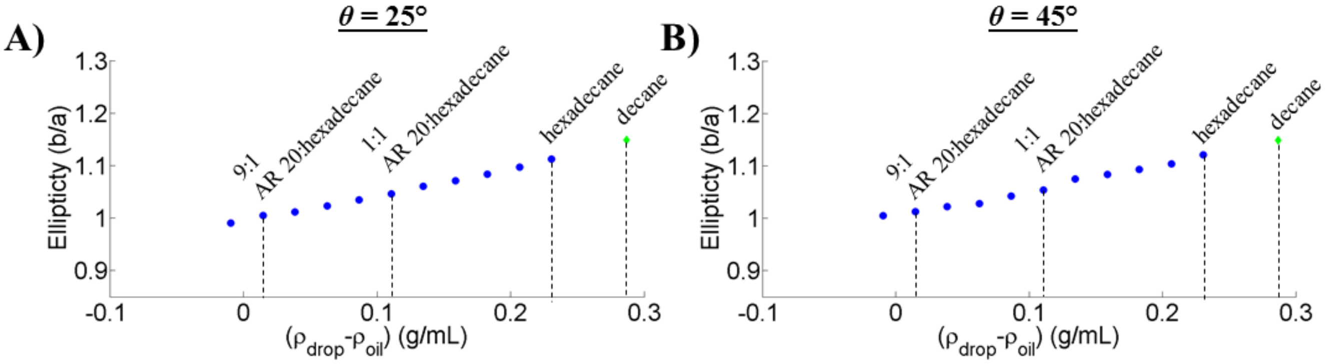

**Figure S5.** Ellipticity as a function of the difference in droplet and oil density. Ellipticity values are computed based on the major and minor axis diameters calculated using coordinates of the interface after Surface Evolver trials. (A) and (B) are drawn from Surface Evolver trials using identical parameters except for the equilibrium contact angle. A) θ=25°. B) θ=45°. The density differences associated with oil compositions included in the manuscript are labeled. Blue circles represent values obtained by varying the volume fraction (% vol) of AR 20 in an AR 20:hexadecane mixture. The green diamond represents pure decane.

## EFFECTS OF SURFACE TENSION ON ELLIPTICITY

Monolayer tension values provided in the manuscript (Table 1) fall between 1.03 and 1.42 mN/m. These results are based on specific capacitance trials in which area is corrected by the factors in Table S2, and these factors were obtained from Surface Evolver trials using a value of 1 mN/m as the input monolayer tension. To investigate the possibility that ellipticity changes significantly with increasing monolayer tension, Surface Evolver trials are performed for a range of monolayer tension values. The droplet volume is set to 300 nL, and the oil type is set as pure hexadecane where gravitational effects are most significant. Figure S6 shows calculated values for ellipticity as a function of the input monolayer tension. Figure S6 shows that the major axis of the interface is about 11% longer than the minor axis at 1 mN/m ($\varepsilon$=1.11). Increasing tension to 1.5 mN/m reduces the ratio $\varepsilon=b/a$ to 1.07, thus the cases with 1.4 mN/m tensions would require < 3-4 % change in the ellipticity factor. For the cases tested here, it thus seems reasonable to use the single set of ellipticity factors obtained from the Surface Evolver data using 1 mN/m as the input monolayer tension.

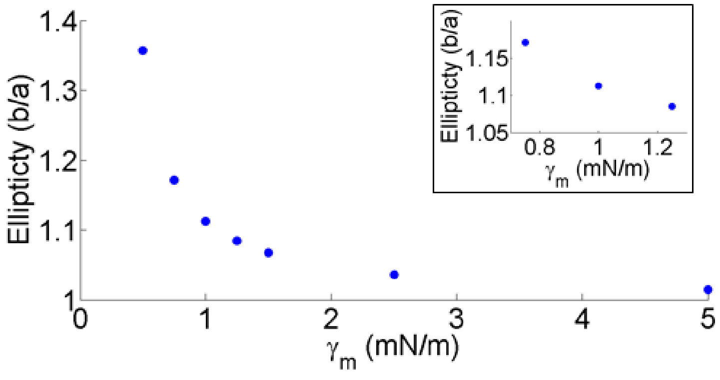

**Figure S6.** Ellipticity as a function of input monolayer tension obtained from Surface Evolver trials with 300 nL droplets in pure hexadecane. The inset highlights the region of monolayer tension values encountered experimentally in this work (~1.0 mN/m).

**Table S2.** Table of Ellipticity Factors by Oil Type

| **Oil** | **Correction Factor, Ellipticity (b/a)** |
|---|---|
| Decane | 1.232 |
| Hexadecane | 1.158 |
| 1-1 AR20:Hexadecane | 1.045 |
| 9-1 AR20:Hexadecane | 0.990 |

## UNCERTAINTY AND ERROR PROPAGATION IN TENSION MEASUREMENTS

Monolayer tension ($\gamma_m$) measurement requires independently obtained values for both $C_M$ and $m$ (refer to Equations 1 and 2 in the manuscript for more context).

$$\gamma_m = \frac{C_M}{4m} \quad \text{Equation S5}$$

The uncertainty in tension measurement thus involves uncertainty of both specific capacitance measurements and the measured values of *m*. We are able to define the sensitivity index $\Omega$ for each contributor.

$$\Omega_{C_M} = \frac{\partial \gamma_m}{\partial C_M} \quad \text{Equation S6}$$

$$\Omega_m = \frac{\partial \gamma_m}{\partial m} \quad \text{Equation S7}$$

Total uncertainty, $u_R$, is obtained as the square root of the sum of the square of each contributing sensitivity index multiplied by the uncertainty in the respective independent variable ($u_{C_M}$ and $u_m$).

$$u_{\gamma_m} = \pm\sqrt{(\Omega_{C_M} u_{C_M})^2 + (\Omega_m u_m)^2} \quad \text{Equation S8}$$

The uncertainty in each independent variable is computed using the student t-test factor ($t_{n,p;}$ *n* is the number of samples and *p* is the probability level) and the standard deviation ($\sigma$) for each respective measurement method.

$$\begin{aligned} u_{C_M} &= \pm t_{n,95}\sigma_{C_M} \\ u_m &= \pm t_{n,95}\sigma_m \end{aligned} \quad \text{Equation S9}$$

The overall uncertainty of monolayer tension measurements is then calculated using Equation 4, Equation 5, and differentiating Equation 1 to obtain expressions for $\Omega$.

$$u_{\gamma_m} = \pm\sqrt{\left(\frac{1}{4m}u_{C_M}\right)^2 + \left(\frac{-C_M}{4m^2}u_m\right)^2} \qquad \text{Equation S10}$$

The average and standard deviation from $C_M$ and $m$ calculations are 0.652±0.027 $\mu F/cm^2$ and 1.41±0.158 $V^{-2}$, respectively (DPhPC in hexadecane data). The resulting value for overall uncertainty in measuring monolayer tension is $u_{\gamma_m} = \pm 0.316$ mN/m. This is roughly equivalent to the uncertainty estimated simply by $u_{\gamma m} = \pm t_{n,95}\sigma_{\gamma m}$ (standard deviation for DPhPC monolayer tension is 0.136 mN/m).

Uncertainty in bilayer tension ($u_{\gamma_b}$) can be approximated using the same approach described for monolayer tension, although Equation 1 is replaced by the Young equation defining bilayer tension. The independent variables are $\gamma_m$ and $\theta$. The contribution from monolayer tension measurements, $u_{\gamma_m}$, is calculated above. The standard deviation of $\theta$ measurements made on a group of images is found in the manuscript to be 0.768°. Using the average angle of 29.3°, the overall uncertainty including propagation of error in $\gamma_m$ and $\theta$ is 1.813 mN/m. Clearly this is greater than the standard deviation observed with bilayer tension values provided in Table 1 in the manuscript. As with monolayer tension above, a more reasonable estimate of bilayer tension measurement uncertainty is obtained by $u_{\gamma b} = \pm t_{n,95}\sigma_{\gamma b}$ = (2.306)(0.222) = ±0.512 mN/m ($n$=8).

## CONTACT ANGLE VARIATION THROUGH MECHANICAL MANIPULATION

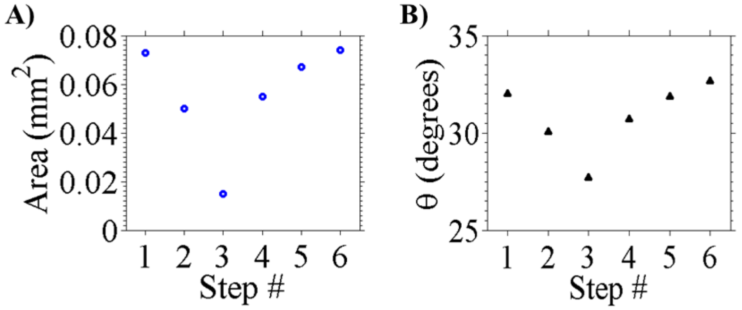

**Figure S7.** (A) Area and (B) contact angle at each step during Part 2 of the DPhPC DIB experiment shown in Fig. 5A-B in the manuscript. With each step, area is either decreased or increased by changing the distance between electrodes. Generally, contact angle is seen to increase with increasing bilayer area and vice versa (see also Fig. 5 and related discussion in the manuscript).

## EFFECTS OF INITIAL, ZERO-VOLT CONTACT ANGLE WITH YOUNG-LIPPMANN

The Young-Lippmann equation can be used to predict the contact angle in response to applied voltage assuming that specific capacitance ($C_M$), monolayer tension ($\gamma_m$), and the zero-volt contact angle ($\theta_0$) are known. Rearranging Equation 3 in the manuscript yields

$$\theta_V(V) = \cos^{-1}\left(cos(\theta_0) - \frac{C_M}{4\gamma_m}V^2\right). \qquad \text{Equation S11}$$

Fig. S8A shows theoretical $\theta_V$ as a function of voltage across the range of 0-300 mV for various initial contact angles ($\theta_0$= 5°, 15°, 25°, 35°, 45°). $C_M$ and $\gamma_m$ values used in the calculations are taken from Table 1 in the manuscript (for DPhPC in hexadecane). The data in Fig. S8A can be used to compute the nominal change in the contact angle ($\Delta\theta$) in response to voltage for each zero-volt angle case using

$$\Delta\theta(V) = \theta_V(V) - \theta_0. \qquad \text{Equation S12}$$

Fig. S8B shows $\Delta\theta$ for each zero-volt angle case shown in Fig. S8A. For a given applied voltage, the magnitude of the nominal change in $\theta$ depends on $\theta_0$. For instance, 300mV results in a 24° change when $\theta_0$ = 5° while the same voltage results in <10° change when $\theta_0$ = 45°. Notably with DIBs, typical values for $\theta_0$ are closer to 25-35°, although it is clear that the zero-volt contact angle can be an important parameter affecting the electrowetting response described by the Young-Lippmann equation.

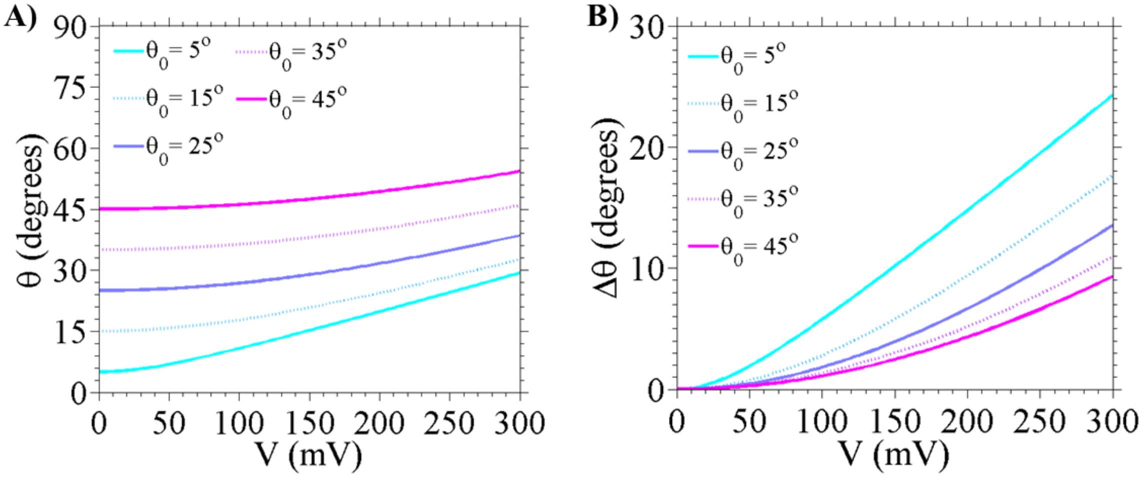

**Figure S8.** A) Theoretical contact angle predicted by the Young-Lippmann equation for various hypothetical zero-volt contact angles ($\theta_0$) with a DPhPC DIB formed in hexadecane ($C_M$ = 0.65 μF/cm$^2$, $\gamma_m$ = 1.18 mN/m). The simulated input voltage is linearly varied across the range from 0-300 mV. B) Data in (A) converted to show the change in contact angle ($\Delta\theta$) with increasing applied voltage.

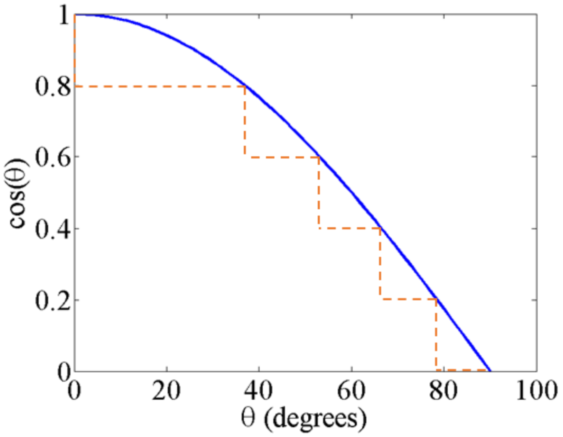

**Figure S9.** The solid line shows cos($\theta$) across the range of $\theta = 0°$ to $90°$. The dashed line shows unitary stepwise (vertical) decreases in cos($\theta$) and the associated (horizontal) increase in nominal $\theta$.

Figures S10A-B shows actual capacitance and area data collected at 12.5 mV intervals between 0 and 175 mV in electrowetting trials beginning from one of two zero-Volt contact angles. The variation in $\theta_0$, as before, is achieved via mechanical manipulation. The data in Fig S10A-B can be reduced to a single plot for comparison by normalizing capacitance and area by their initial zero-Volt values. The resulting behavior can be described by

$$C/C_0 = 1 + \alpha V^2, \qquad \text{Equation S13}$$

and

$$A/A_0 = 1 + \beta V^2, \qquad \text{Equation S14}$$

where $\alpha$ and $\beta$ are parameters that describe the sensitivity of interface to capacitance and area increases, respectively, in response to increasing applied voltage and electrowetting. The data in Fig. S10A-B can be normalized by the zero-Volt C and A values and plotted as a function of the square of applied voltage as presented in Fig S10C. Linear least squares regression of the curves in Fig. S10C return slope values equal to $\alpha$ and $\beta$ for each case. For both initial contact angle cases, we see that capacitance and area are linear with respect to the square of applied voltage as expected from Equations S13 and S14. The fact that $C/C_0$ and $A/A_0$ curves for a given initial contact angle are almost overlapping is a result of the fact that $C_M$ is not significantly affected by voltage.[4] However, the data in Fig. S10C shows that $\alpha$ and $\beta$ are affected by initial contact angle imposed by varying electrode separation and droplet positioning. Specifically, we see higher values for both $\alpha$ and $\beta$ when beginning at lower zero-Volt contact angles (i.e. droplets pulled

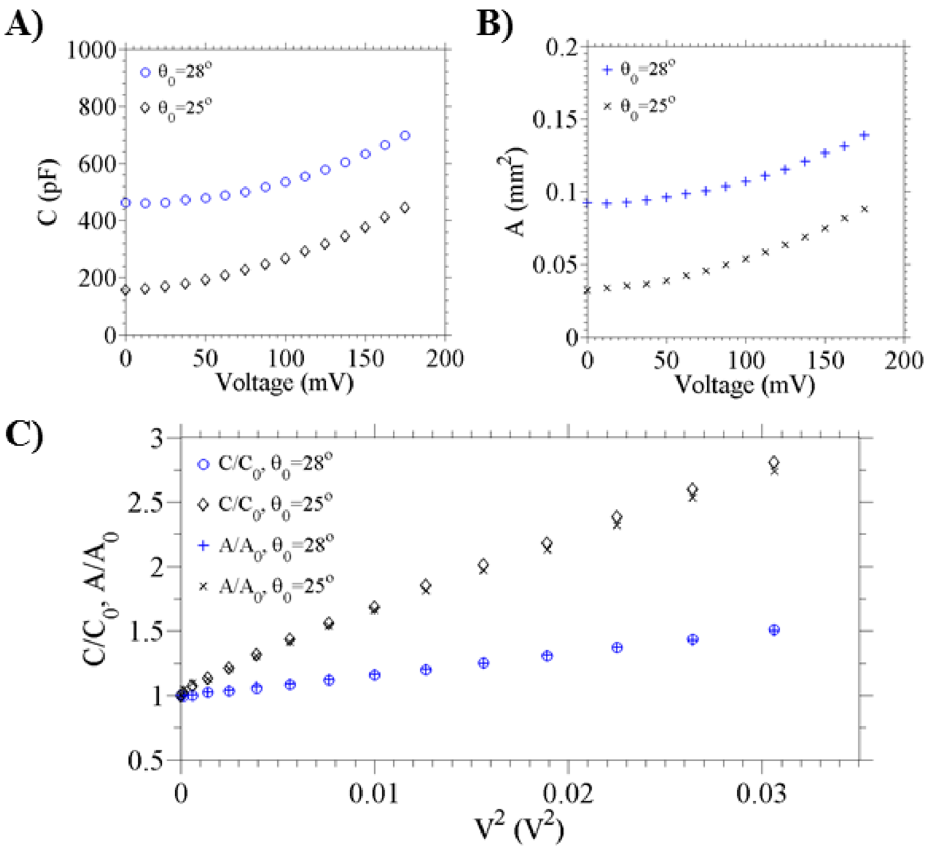

**Figure S10.** A-B) Capacitance and area, respectively, as a function of voltage with two DIBs with varying initial, zero-Volt contact angle. C) Capacitance and area data in (A-B), normalized by the zero-volt capacitance and area, respectively, and plotted against the square of applied voltage.

apart slightly from equilibrium) which is in direct agreement with larger theoretical and experimentally observed changes in the nominal contact angle when starting at lower zero-Volt angles.

## MEASURING VOLTAGE-DEPENDENCE OF SPECIFIC CAPACITANCE

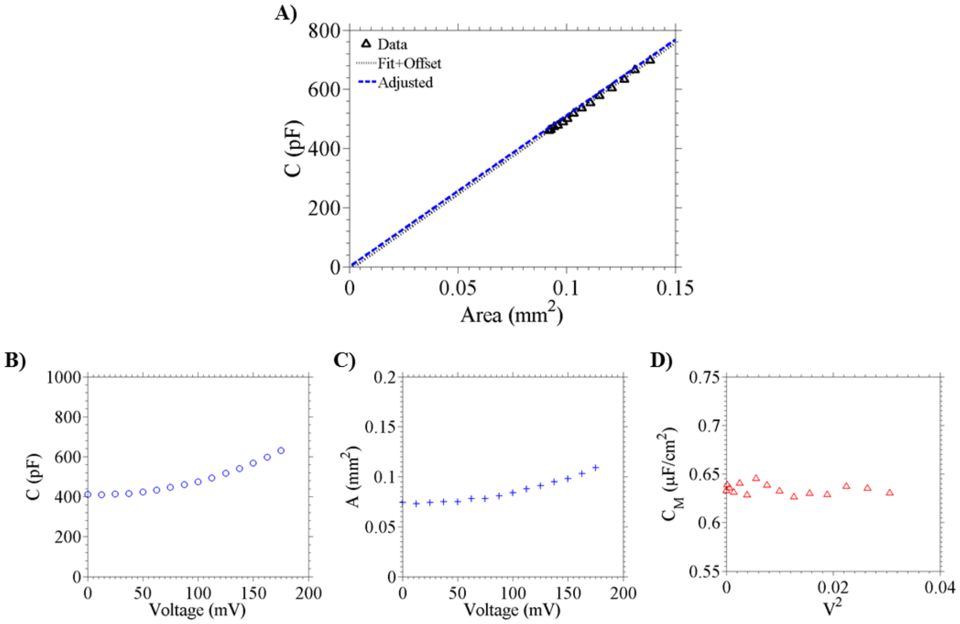

**Figure S11.** A) Actual C versus A data obtained during specific capacitance measurement along with the fit obtained from linear least squares regression (dotted, black) of C versus A. The raw fit displays a small capacitance offset (y intercept) when A=0. Removing the -11.7 pF offset adjusts the fit (dashed, blue) and can be used to correct. B-D) Electrowetting to measure voltage-dependence of $C_M$ from 0-175mV. (B) and (C) show capacitance (offset removed) and area measured at each voltage step, respectively. D) $C_M$ at each voltage step calculated discretely using C and A data in (B-C).

**Table S3.** Molar Volumes of DPhPC Acyl Chains, Decane, Hexadecane

| **Species** | **Molar Volume [cm$^3$/mol]** | **Ref.** |
|---|---|---|
| DPhPC acyl chains (tetramethyl hexadecanoic acid) | 444.8 | 1 |
| Decane | 194.7 | - |
| Hexadecane | 294.1 | 2 |

## LIPID/SOLVENT MOLAR VOLUME RATIO CALCULATIONS

Estimation of the molar volume ratio of lipid acyl chains to solvent molecules involves the molar volumes of the lipids and solvents as displayed in Table S3. Where available, a source for each value is included in the table. The referenced value for hexadecane is in close agreement with the value obtained simply by dividing the solvent molecular weight by the solvent density to obtain a molar volume with units of [$cm^3$/mol]. Thus the value listed for decane is calculated simply using the density (0.731 g/$cm^3$) and molecular weight (226.45 g/mol) of decane. Note that the value listed for DPhPC, based on the molecular volume provided by the LIPID MAPS database[1] for a single tetramethyl hexadecanoic acid molecule, is converted to molar volume and doubled to account for two acyl chains on each DPhPC lipid molecule.

Results provided in the manuscript are based on previous estimates[4] that with DPhPC DIBs formed in hexadecane solvent, approximately 10% of the hydrophobic region volume consists of the hexadecane solvent. Thus, for any given volume of the hydrophobic bilayer region, a volume ratio of 9:1 exists for lipid acyl chains:solvent. Dividing each value in the ratio by the molar volume then provides a molar ratio of acyl chains: solvent (note: the calculations here include the assumption of two acyl chains per lipid). It then follows that if 10% of the hydrophobic region volume consists of hexadecane solvent, the molar ratio of lipid:solvent falls around 6:1, which means that there is one solvent molecule for every 6 lipids. Consistent with previous findings, results provided in the manuscript suggest that DPhPC DIBs formed in decane contain 43% decane solvent by volume. Conversion from a 53:47 volume ratio of lipid:decane to percent molar volume provides an estimate of 0.58:1 (or 1:1.7). Thus it appears that when DPhPC DIBs are formed in decane, the hydrophobic region contains approximately two solvent molecules for every lipid molecule. These calculations assume that the molar volumes of each component are fixed quantities.

## REFERENCES

1. M. Sud, E. Fahy, D. Cotter, A. Brown, E. A. Dennis, C. K. Glass, A. H. Merrill Jr, R. C. Murphy, C. R. H. Raetz, D. W. Russell and S. Subramaniam, *Nucleic Acids Research*, 2007, **35**, D527-D532.
2. C. M. Hansen, *Hansen Solubility Parameters: A User's Handbook, 2nd Edition*, 2nd edn., CRC Press, Boca Raton, FL, 2007.
3. G. Valincius, F. Heinrich, R. Budvytyte, D. J. Vanderah, D. J. McGillivray, Y. Sokolov, J. E. Hall and M. Lösche, *Biophysical Journal*, 2008, **95**, 4845-4861.
4. L. C. M. Gross, A. J. Heron, S. C. Baca and M. I. Wallace, *Langmuir*, 2011, **27**, 14335-14342.
5. K. A. Brakke, *Experimental mathematics*, 1992, **1**, 141-165.
6. D. Weaire and S. Hutzler, *The physics of foams*, Clarendon Press, 1999.